Combustion and Flame

Role of ammonia addition on polycyclic aromatic hydrocarbon growth: A ReaxFF molecular dynamics study

--Manuscript Draft--

Manuscript Number:	CNF-D-22-00565
Article Type:	Full Length Article
Keywords:	Ammonia; PAHs; Molecule dynamics; Quantum chemistry; HACA pathway; Soot; Carbon-free
Corresponding Author:	Qian Mao University of Duisburg-Essen Duisburg, GERMANY
First Author:	Yunfeng Xu
Order of Authors:	Yunfeng Xu
	Qian Mao
	Ying Wang
	Kai H. Luo
	Lei Zhou
	Zhanyuan Wang
	Haiqiao Wei
Abstract:	Ammonia (NH3), one of the most promising carbon-free fuels, has received great research interest. In particular, NH3 is often blended with hydrocarbon fuels to achieve desired combustion characteristics. However, NH3 addition could affect soot formation, which has not been adequately understood. In this study, the effect of NH3 on the growth of polycyclic aromatic hydrocarbons (PAHs) is investigated with the reactive force field molecule dynamics (ReaxFF MD) simulations and quantum chemistry calculations. The simulation results indicate that NH3 addition slows down the growth of large carbon-containing species in the C2H4/O2 system. Novel path with HCN addition is discovered in the PAH growth, which inhibits the PAH growth compared to the conventional Hydrogen-Abstraction-Carbon-Addition (HACA) path via C2H2 addition. Moreover, quantum chemical calculations verified the rationality of this addition path and explained its inhibition on PAH growth by calculating the heat of reactions and reaction energy barriers. According to the present study, NH3 also has an inhibitory effect on both the HCN addition path and C2H2 addition path by providing H atoms to promote the generation of PAH radicals back to PAH molecules, and this effect is more significant for the C2H2 addition path. Results from the study provide a fundamental insight for the inhibition of PAH growth due to the NH3 addition from an atomistic insight, which helps to improve the understanding of the combustion of blends of NH3 and hydrocarbon fuels.
Suggested Reviewers:	Yihua Ren y.ren@itv.rwth-aachen.de
	Adri van duin acv13@psu.edu
	Fengshan Liu fengshan.liu@nrc.ca
	Lei Zhu tonyzhulei@sjtu.edu.cn

Role of ammonia addition on polycyclic aromatic hydrocarbon growth: A ReaxFF molecular dynamics study

Yunfeng Xu[1], Qian Mao[2,*], Ying Wang[1], Kai H. Luo[3], Lei Zhou[1,*], Zhanyuan Wang[1], Haiqiao Wei[1]

1, State Key Laboratory of Engines, Tianjin University, Tianjin 300072, China;

2, Institute of Technology for Nanostructures, University of Duisburg-Essen, Duisburg 47057, Germany

3, Department of Mechanical Engineering, University College London, Torrington Place, London WC1E 7JE, UK

*Corresponding author:

Email: qian.mao@uni-due.de (Qian Mao)

lei.zhou@tju.edu.cn (L. Zhou)

Abstract

Ammonia (NH_3), one of the most promising carbon-free fuels, has received great research interest. In particular, NH_3 is often blended with hydrocarbon fuels to achieve desired combustion characteristics. However, NH_3 addition could affect soot formation, which has not been adequately understood. In this study, the effect of NH_3 on the growth of polycyclic aromatic hydrocarbons (PAHs) is investigated with the reactive force field molecule dynamics (ReaxFF MD) simulations and quantum chemistry calculations. The simulation results indicate that NH_3 addition slows down the growth of large carbon-containing species in the C_2H_4/O_2 system. Novel path with HCN addition is discovered in the PAH growth, which inhibits the PAH growth compared to the conventional Hydrogen-Abstraction-Carbon-Addition (HACA) path via C_2H_2 addition. Moreover, quantum chemical calculations verified the rationality of this addition path and explained its inhibition on PAH growth by calculating the heat of reactions and reaction energy barriers. According to the present study, NH_3 also has an inhibitory effect on both the HCN addition path and C_2H_2 addition path by providing H atoms to promote the generation of PAH radicals back to PAH molecules, and this

effect is more significant for the C_2H_2 addition path. Results from the study provide a fundamental insight for the inhibition of PAH growth due to the NH_3 addition from an atomistic insight, which helps to improve the understanding of the combustion of blends of NH_3 and hydrocarbon fuels.

Keywords: Ammonia; PAHs; Molecule dynamics; Quantum chemistry; HACA pathway; Soot; Carbon-free

1. Introduction

The extensive use of fossil fuels in industry and transportation has caused severe environmental problems that are detrimental to human health [1]. To reduce the carbon dioxide (CO_2) emissions from the combustion of the hydrocarbon fuels, carbon-free fuels like hydrogen (H_2), ammonia (NH_3) are regarded as promising alternatives and have attracted much attention. In comparison to H_2, NH_3 is a preferable choice because it is often in liquid phase rather than gas phase, which makes it easier to transport and store. Another advantage of NH_3 is its low cost per unit of stored energy and high volumetric energy density (7.1–2.9 MJ/L) [2] However, because of its low laminar burning velocities and unstable flames, NH_3 is not a viable alternative fuel [3] on its own. Therefore, a hybrid combustion approach of NH_3 with hydrocarbon fuels such as methane (CH_4) or ethylene (C_2H_4) has been proposed and has proven to be a promising solution[4, 5].

The combustion properties of NH_3 and its hydrocarbon blends, particularly in CH_4-NH_3 flames, have been extensively studied, and majority of them concentrated on flame characteristics [6, 7], NO_X and CO_2 emissions [8, 9]. In addition, addition of NH_3 is found to influence the PAH and soot formation in flames. Matthew et al. [10] investigated the soot formation of CH_4/ NH_3 blend flames and discovered that the C_2H_2 concentrations in the CH_4/ NH_3 blend flames decreased marginally, along with a considerable suppression of benzene. With NH_3 addition up to 20% or more, the soot volume fraction was reduced by more than a factor of 10. Existing chemical kinetic mechanisms [11] can accurately capture the soot concentration in CH_4 flames, but not in NH_3/CH_4 flames, highlighting the need for better chemical kinetic mechanisms to

forecast soot formation in ammonia-hydrocarbon blend flames. Shao et al. [12] investigated the inhibitory effect of NH_3 addition on the soot formation in C_2H_4 flames, and found that doping with NH_3 in the C_2H_4 flame reduced both soot particle size and the soot volume fraction. Chemical kinetic analysis indicated that C-N species generated in C_2H_4/NH_3 flames can inhibit carbon from participating in soot precursor formation, resulting in less soot formation. Renard et al. [13] discovered that adding NH_3 to C_2H_4 flames had a minor effect on the C_2H_2 concentrations but a significant effect on C_5-C_{10} intermediates. Bennett et al. [14] investigated the soot formation in a laminar counterflow flame with C_2H_4 fuel mixed with different proportions of NH_3, and discovered that the effect of NH_3 addition was not apparent for the formation of naphthalene ($C_{10}H_8$), whereas it started to become significant for larger PAHs. In addition, HCN is a crucial intermediate in NH_3 combustion. Haynes et al. [15] suggested the inhibitive effect on soot concentrations may be due to a quantitative formation of HCN. However, the effect of NH_3 and its byproduct (HCN) on soot formation is still not well understood, and the detailed chemical reaction paths of PAH growth with NH_3 or HCN addition are still controversial.

The goal of the present study is to conduct a theoretical study to systemically explore the chemical effect of NH_3 and its byproduct HCN on the PAH growth from an atomistic perspective Firstly, the intermediate species are analyzed for NH_3 addition to the C_2H_4/O_2 system. Then, the effects of HCN and C_2H_2 addition to naphthyl ($C_{10}H_7$•) in terms of the PAH growth are discussed from the reaction paths. Finally, NH_3 addition on the PAH growth is discussed.

2. Methodology

2.1 ReaxFF force field

The ReaxFF MD was developed to bridge the gap between quantum chemistry and classical MD simulation [16], which enables the simulation of reactive systems. The ReaxFF, as a function of the bond order, is expressed in Eq. (1), where terms on the right-hand-side of the equation represent bond energy, over-coordination energy

penalty, under-coordination stability, lone pair energy, valence angle energy, torsion angle energy, Coulomb energy, and van der Waals energy [17]. A more detailed description of the ReaxFF formulation can be found in the work by van Duin et al. [18].

$$E = E_{bond} + E_{over} + E_{under} + E_{lp} + E_{val} + E_{tor} + E_{coul} + E_{vdw} \quad (1)$$

Currently, there are 9 sets of ReaxFFs describing interactions of C/H/O/N in literature. To figure out the most suitable set of force field for the NH_3 and hydrocarbons, we performed MD simulations of CH_4/ NH_3 blend oxidation with all the available 9 sets of force fields as shown in Fig. S1 in Supplemental Material. The time evolutions of the consumption of CH_4 and NH_3 at both 2000 and 3000 K were calculated with the same initial component mole fraction in the experiment [19]. Since the bond dissociation energies (BDEs) of NH_3 and CH_4 are 435 kJ/mol and 431 kJ/mol [20, 21], respectively, as shown in Fig. 1(a), the molecular stability and reactivity of NH_3 and CH_4 should be similar. Among all the 9 sets of force fields, the C/H/N/O force field from Kulkarni et al. [22] can well capture the trend of CH_4 and NH_3 changes as shown in Fig. 1(b) as the consumption rate of both CH_4 and NH_3 are almost the same, which agree with the similar BDEs of CH_4 and NH_3, as well as that from the experimental measurements of the species concentration in the NH_3/ CH_4 low-pressure flame by Tian et al [19]. Therefore, the ReaxFF force field from Ref. [22] is selected in the present study to describe the reactions of NH_3 and hydrocarbons.

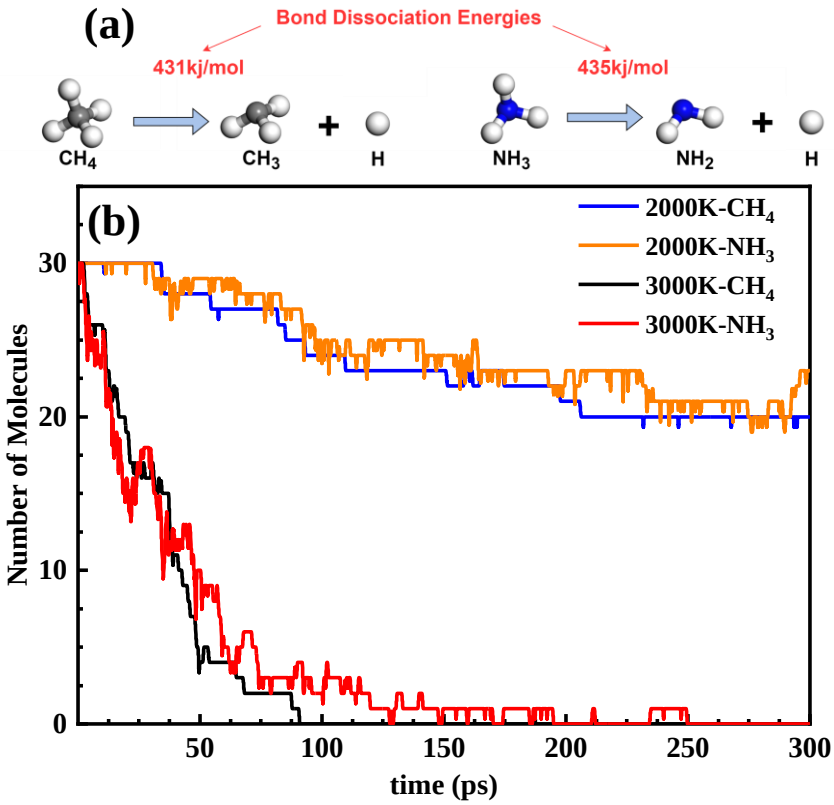

Fig. 1. (a). Bond dissociation energies of NH_3 and CH_4. (b). Time evolution of CH_4 and NH_3 molecules in the CH_4/ NH_3/ O_2 system at 2000 and 3000 K, respectively.

2.2 MD simulations

To study the effect of NH_3 addition on the growth process of C-containing species in the system during the combustion of hydrocarbon fuels, a series of simulations with different initial settings are conducted, as shown in Table 1. Since ethylene (C_2H_4) has a moderate sooting tendency and is usually a common choice for base soot studies [23], we selected C_2H_4 as the basic fuel for this study. To describe the amount of NH_3 added to the C_2H_4 system, the NH_3 addition ratio (α) is defined as the ratio of the number of NH_3 molecules, n (NH_3), to the number of ethylene molecules, n (C_2H_4), as shown in Eq. (2). The density of each system is kept the same at 0.3 g/cm^3 by varying the size of the computational box. According to Bennett et al.'s [14] experiments, the inhibitory of NH_3 addition on soot formation was mainly in PAHs larger than $C_{10}H_8$. Therefore, the reactivity of NH_3, HCN and C_2H_2 addition to naphthyl radicals ($C_{10}H_7$•) and the

follow-up PAH growth are extensively studied in this present study. Details of the simulation setup are listed in Table 2.

$$\alpha = n(NH_3)/n(C_2H_4) \quad (2)$$

The simulations are performed under the canonical ensemble (NVT), and the temperature is controlled via the Nosé–Hoover thermostat. The simulations are conducted at 3000 K for 500 ps. The periodic boundary condition is implemented in the three directions. The bond order cutoff is set to be 0.3 and the time step is 0.1 fs.

All the ReaxFF MD simulations are carried out with the REAXC package in the Large-scale Atomic/Molecular Massively Parallel Simulation (LAMMPS). The reaction paths are obtained by Chemical Trajectory AnalYzer (ChemTraYzer) scripts [24]. The dynamic trajectories were visualized using Visual Molecular Dynamics (VMD) software [25].

Table 1
Simulation conditions of the C_2H_4 system

	n(C_2H_4)	n(O_2)	n(NH_3)	α
System 1	200	600	0	0
System 2	200	600	100	0.5
System 3	200	600	200	1

Table 2
Simulation conditions of the $C_{10}H_7$ system

	n($C_{10}H_7$)	n(HCN)	n(C_2H_2)	n(NH_3)
System 4	50	500	0	0
System 5	50	250	250	0
System 6	50	0	500	0
System 7	50	0	250	250
System 8	50	0	0	500
System 9	50	250	0	250

2.3 Quantum chemical calculations

To further validate to results of PAH growth via HCN and C_2H_2 addition from ReaxFF MD simulations. The potential energy surfaces of HCN and C_2H_2 addition to naphthyl are computed with density functional theory (DFT). The optimized geometries of all stationary points on the $C_{10}H_7$ + HCN/C_2H_2potential energy surfaces were obtained using the M06-2X [26] method with the 6-311+G (d, p) basis set. The vibrational frequencies and zero-point energies (ZPEs) were calculated at the same level. The DFT calculations were conducted with ultrafine grid and ultra-tight convergence criteria. Species on the PES are ensured to be the minimum energy conformers. The accuracy of the M06-2X method for the study of PAHs has been reported before [27, 28]. The M06-2X calculations were performed using the Gaussian 09 program package [29].

3. Results and discussion

In this section, we firstly discuss the effect of NH_3 addition on intermediates formation in C_2H_4/O_2 systems under different NH_3 addition ratios, and then explore the effect of NH_3 and HCN addition to the $C_{10}H_7$ radicals compared against the traditional C_2H_2 addition on the PAH growth.

3.1 Effect of NH_3 addition in C_2H_4/ O_2 systems

To investigate the effect of NH_3 addition on the growth process of C-containing species in the system during the combustion of hydrocarbon fuels, simulations were performed with different NH_3 addition ratios (α) in the C_2H_4/O_2 system. Figure 2(a) shows the temporal evolution of the total number of C_1 and C_2 (donated as C_{1-2}), as well as C_3 and larger species (donated as C_{3+}) at different α at 3000 K. It is found that with the increase of NH_3 addition, more C_{1-2} species were formed, and the amount of C_{3+} species is reduced. This indicates that NH_3 addition inhibits the formation of large carbonous species in the C_2H_4/O_2 system. It can also be confirmed by the structures of the largest species formed within 500 ps as shown in Fig. 2(b). The structures of the

largest species are $C_8H_4O_5$, C_5H_7NO and $C_5H_4NO_2$ for α = 0, 0.5 and 1, respectively. This indicates the largest species size decreases with the NH_3 addition.

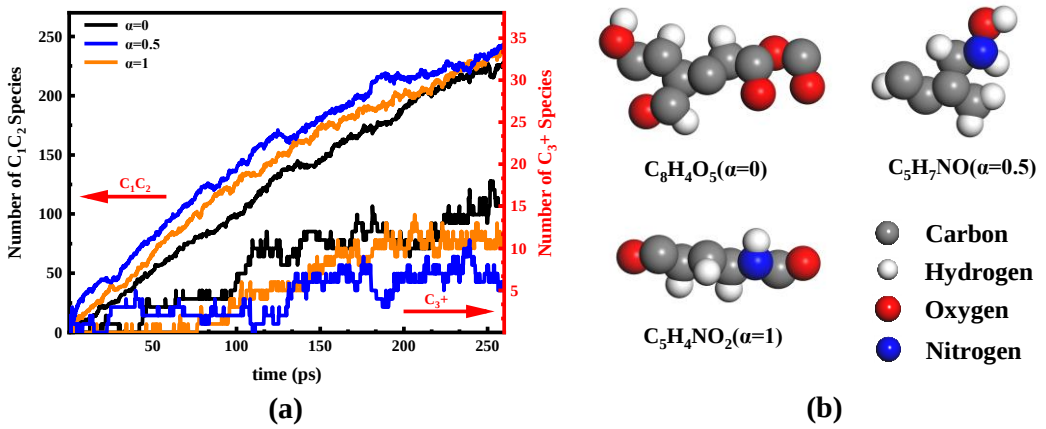

(a) (b)

Fig. 2 (a). Time evolutions of C_1C_2 and C_3+ species in C_2H_4/ O_2 systems with different NH_3 addition ratios α. (b). The largest species generated by the system within 500 ps.

According to the observation of the product evolution in systems 1 to 3, the effect of NH_3 addition on the growth of hydrocarbons in the C_2H_4/O_2 system can be depicted by Fig 3(a). The complex interactions between NH3 and the small hydrocarbon radicals produce some C-N species like HCN, preventing the C atoms in the system from producing larger C-H species. Consequently, the formation of soot is slowed down. In this process, HCN is an important intermediate product, and more HCN production is also found in the MD simulations, as shown in Fig. 3(b). However, compared to soot, the emission of HCN is more concerning [30], as it poses a significant threat to the human health such as pneumonia, bronchitis and susceptibility to virus infections. Understanding its generation mechanism can help to effectively control the generation of HCN. Therefore, routes of HCN formation in $C_2H_4/O_2/NH_3$ systems are further investigated, and it mainly results from following three routes as shown in Fig. 3(c). The first route is from the reaction of C_2H_4 and C_2H_3O to form C_4H_7O, then occurs a series of cracking and dehydrogenation reactions to form CH_3. CH_3 combines with NH_2 to form CH_3-NH_2, which subsequently leads to HCN through the dehydrogenation reactions. The second route initiates from the C_2H_2O and NH_2 recombination reaction,

which then cracks to form CH_4-NH, and dehydrogenates to HCN eventually. The third route begins with the reaction of CO and NH_2 and forms intermediate species of NH_2CO, which then converts to HCN via a series of complex reactions as indicated in Fig. 3(b).

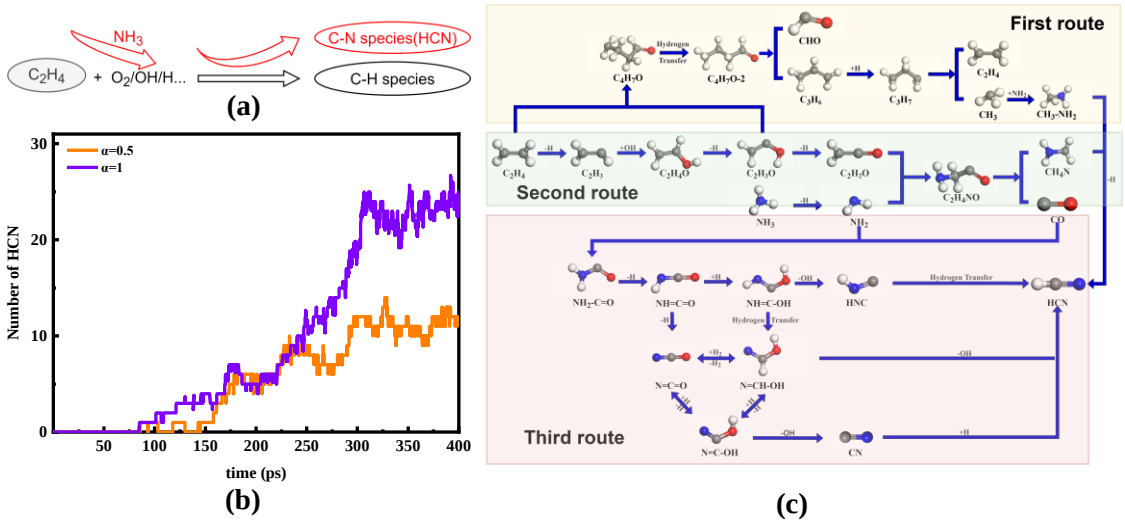

Fig. 3 (a).Diagram of the effect of NH_3 addition on the growth of hydrocarbons in the C_2H_4/O_2 system. (b).Time evolutions of HCN molecules. (c).The routes of HCN generation in system 2 (containing 200 C_2H_4 molecules, 600 O_2 molecules, and 100 NH_3 molecules).

3.2 HCN and C_2H_2 additions on the PAH growth

HCN has a triple-bond, which share high similarity with C_2H_2. The Hydrogen-Abstraction-Carbon-Addition (HACA) path [31, 32] is widely understood to be critical for the PAH growth. As a result, HCN could potentially participate in the PAH growth and play a competitive role to the traditional HACA path with C_2H_2 addition. Therefore, we performed a series of molecular dynamics simulations and quantum chemical calculations to investigate the role of HCN and C_2H_2 on the growth of PAH.

Figure 4 displays the potential energy surface of HCN and C_2H_2 addition to $C_{10}H_7$ at the M06-2X/6-311+G (d, p) level of theory. The solid and dashed lines depict the energy changes for $C_{10}H_7$-1 and $C_{10}H_7$-2 addition reactions, respectively. For both C_2H_2 and HCN, the energy barrier and heat of reaction for the addition reactions of $C_{10}H_7$-1 are almost identical to that of $C_{10}H_7$-2, implying the reaction kinetics of the two

structures should be similar. As a result, $C_{10}H_7$-1 was chosen as the subject for PAH growth study in ReaxFF MD simulations.

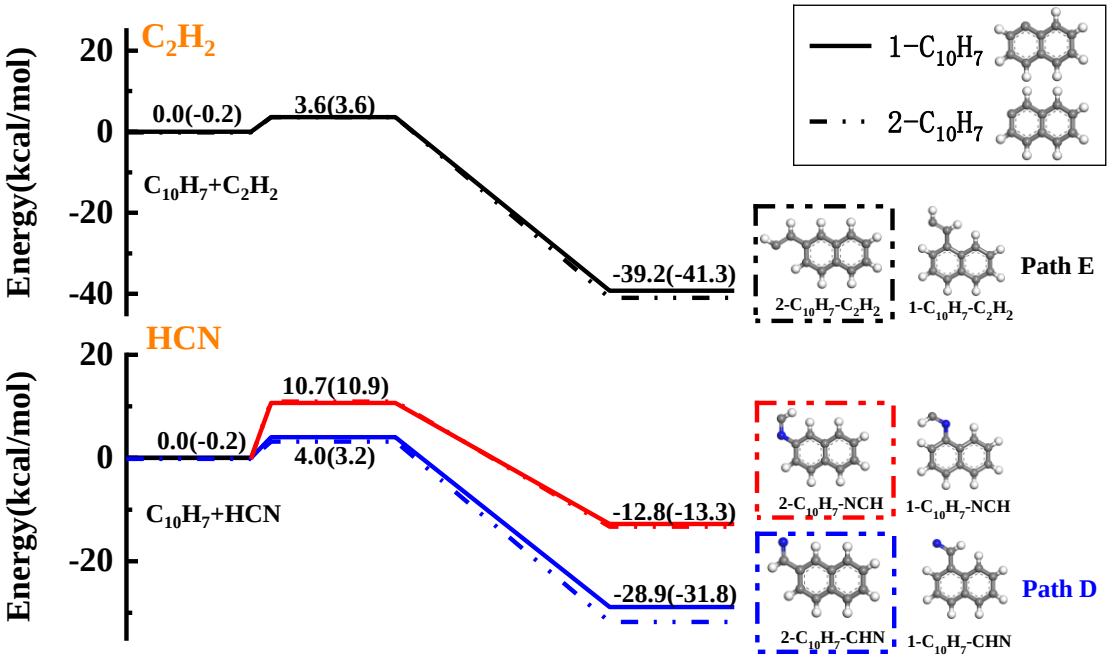

Fig. 4. Potential energy surface of HCN and C_2H_2 addition to $C_{10}H_7$ at the M06-2X/6-311+G (d, p) level of theory.

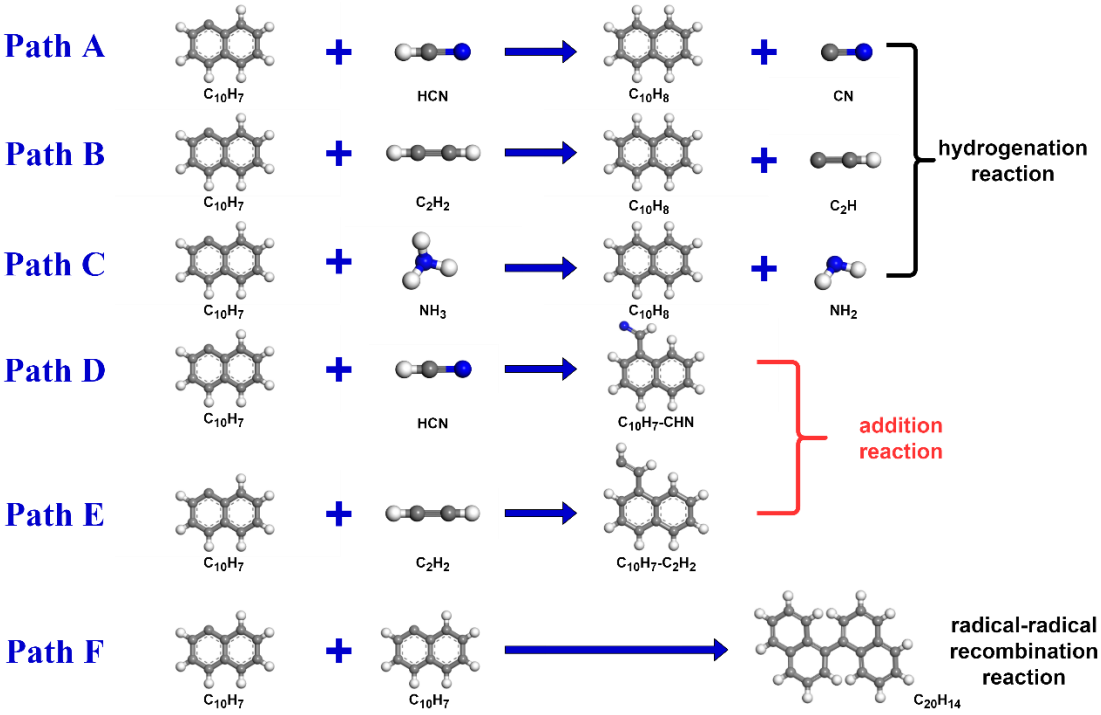

Fig. 5. Reaction paths of 1-naphthyl ($C_{10}H_7$) with HCN, C_2H_2 and NH_3.

The MD simulations in systems 4 to 9 (as shown in Table 2) have been conducted to investigate the growth of PAH with the different addition ratios of HCN/ C_2H_2/ NH_3. Figure 5 shows the main reaction paths. The reactions of $C_{10}H_7$ with HCN/ C_2H_2/ NH_3 can be classified into hydrogenation reaction (Path A, B, and C), addition reaction (Path D, E), and radical-radical recombination reaction (Path F). Among them, hydrogenation and radical-radical recombination reactions occur in all systems, but addition reactions occur only between HCN and $C_{10}H_7$ or between C_2H_2 and $C_{10}H_7$. As the main path for PAH growth, these two addition reactions (Path D and Path E) will be discussed in detail in this section.

To figure out the PAH growth path via the HCN-addition and the C_2H_2 addition, the competitive mechanism of the two paths, the results of systems containing $C_{10}H_7$, C_2H_2 and HCN were analyzed simultaneously. The percentages of different types of reactions are shown in Fig. 6. In system 4 with $C_{10}H_7$ and HCN, addition reactions occur between HCN and $C_{10}H_7$ (Path D). It is noteworthy that the C is preferentially attached to $C_{10}H_7$ instead of N. In terms of molecular geometry of HCN, it is possible for both C, N atoms of HCN adding to $C_{10}H_7$, resulting in two possible structures: $C_{10}H_7$-NCH and $C_{10}H_7$-CHN (as shown in Fig. 4.). However, only one product, $C_{10}H_7$-CHN, was found in the molecular dynamics simulation results. Further analysis of the HCN addition reactions from the quantum chemical calculations, it is found that, the HCN addition to $C_{10}H_7$ with the formation of $C_{10}H_7$-CHN has a lower energy barrier, 4.0kal/mol, compared to that of forming $C_{10}H_7$-NCH at a barrier height of 10.7kal/mol as shown in Fig. 4. Moreover, the product $C_{10}H_7$-CHN is thermodynamically more stable with a lower energy of -28.9kal/mol, while that of the product $C_{10}H_7$-NCH is -12.8kal/mol. These indicate that $C_{10}H_7$ and HCN are more likely to react to produce the product $C_{10}H_7$-CHN. The results of the quantum chemical calculations provide sufficient evidence that only one addition product, $C_{10}H_7$-CHN, was observed in the molecular dynamics simulations, and it also indicates that the force field selected in this study is trustworthy for studying the process of PAH growth.

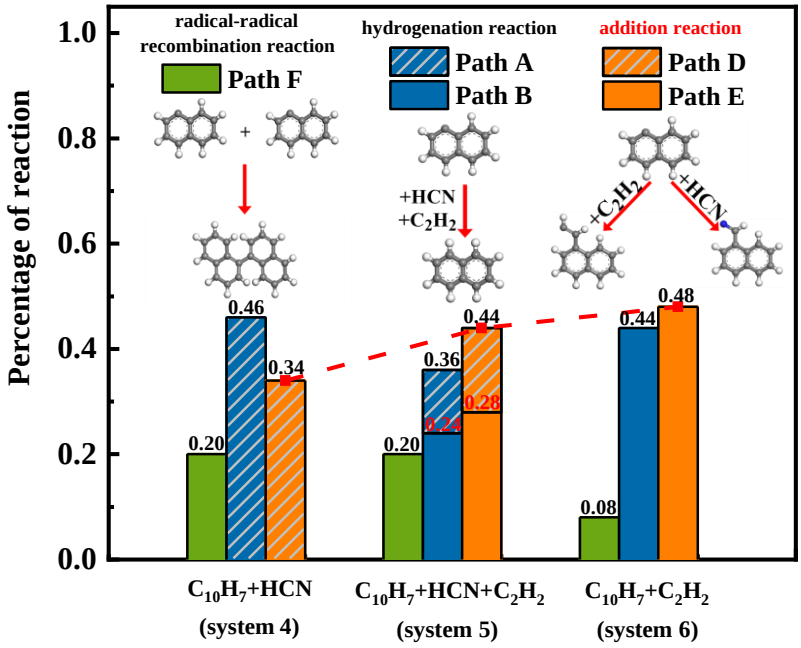

Fig. 6. Percentage of each reaction type in the systems of HCN added to $C_{10}H_7$/ C_2H_2. (Green for radical-radical reactions, blue for hydrogenation reactions and orange for addition reactions, the shaded part for the reaction with HCN, and the un-shaded part for the reaction with C_2H_2.)

The red dashed line in Fig. 6 shows changes of the number of addition reactions. With increasing C_2H_2 molecules in systems 5 and 6, the percentage of addition reactions shows an upward trend. And in system 5 (HCN: C_2H_2=1:1), the percentage of the C_2H_2 addition reaction is higher than that of the HCN addition. This indicates that HCN can react with $C_{10}H_7$ for PAH growth, but with a lower preference than the conventional HACA path. This is confirmed from the results of the quantum chemistry calculations. From the potential energy surface in Fig. 4. The C_2H_2 addition to $C_{10}H_7$ with the formation of $C_{10}H_7$-C_2H_2 has a lower energy barrier, 3.6kal/mol, while the HCN addition to $C_{10}H_7$, forming $C_{10}H_7$-CHN, is at a barrier height of 4.0kal/mol. Moreover, the product $C_{10}H_7$-C_2H_2 is more stable with a lower energy of -39.2kal/mol, while the energy of product $C_{10}H_7$-CHN is -28.9kal/mol compared to reactants. This implies that C_2H_2 addition to $C_{10}H_7$ is more feasible than the HCN addition reactions.

According to the above analysis, the addition of HCN reduces the proportion of the total addition reactions (including both the reactions with HCN and C_2H_2). To validate whether such a phenomenon still exists in the subsequent PAH growth process, simulations with extended simulation time have been performed. Within 500 ps, the

largest species produced in systems 4($C_{10}H_7$/ HCN), 5($C_{10}H_7$/ C_2H_2/ HCN) and 6($C_{10}H_7$/ C_2H_2) are $C_{88}H_{49}N_{17}$, $C_{121}H_{79}N_{10}$ and $C_{177}H_{139}$, respectively. This implies that the addition of HCN inhibits the growth of PAH. Three main reasons are listed below. Firstly, HCN and C_2H_2 compete to react with $C_{10}H_7$, which slows down the whole PAH growth process. Secondly, the structure of $C_{10}H_7$-CHN generated by the addition of HCN to $C_{10}H_7$ is less stable than $C_{10}H_7$-C_2H_2 and has a higher energy barrier, which reduces the growth rate of $C_{10}H_7$ in the whole system. Thirdly, about 28.0% C_2H_2 is consumed by HCN through R1 and R2, which reduces C_2H_2 and HCN species for the $C_{10}H_7$ growth.

$$C_2H_2+HCN \rightarrow C_3H_3N \quad \text{R1}$$

$$C_2H_2+HCN \rightarrow C_2H+CH_2N \quad \text{R2}$$

3.3 Effects of NH_3 addition on conventional HACA-type path and the HCN-added PAH growth path.

Moreover, the effect of NH_3 on the PAH growth is examined. Figure 7(a) shows the percentage of each reaction type in systems 8 ($C_{10}H_7$/NH_3), 4 ($C_{10}H_7$/ HCN) and 9 ($C_{10}H_7$/ HCN/ NH_3). It can be seen that NH_3 addition slightly affects the radical-radical recombination reaction. However, with increasing NH_3 addition, the number of hydrogenation reactions increases, while the number of addition reactions decreases. A similar trend also can be found in the systems of 8 ($C_{10}H_7$/ NH_3), 6 ($C_{10}H_7$/ C_2H_2) and 7 ($C_{10}H_7$/ C_2H_2/ NH_3) as shown in Fig. 7(b). The NH_3 shows an obvious inhibitory effect on the addition reactions for the system containing C_2H_2 (System 7). It can be seen that the slope of the red dashed line in Fig. 7(b) is significantly larger than that in Fig. 7(a). Note that the addition of NH_3 significantly increases the percentage of hydrogenation reactions in the system, which results in the formation of a stable $C_{10}H_8$ structure and finally prohibits addition reactions for the further growth of PAHs.

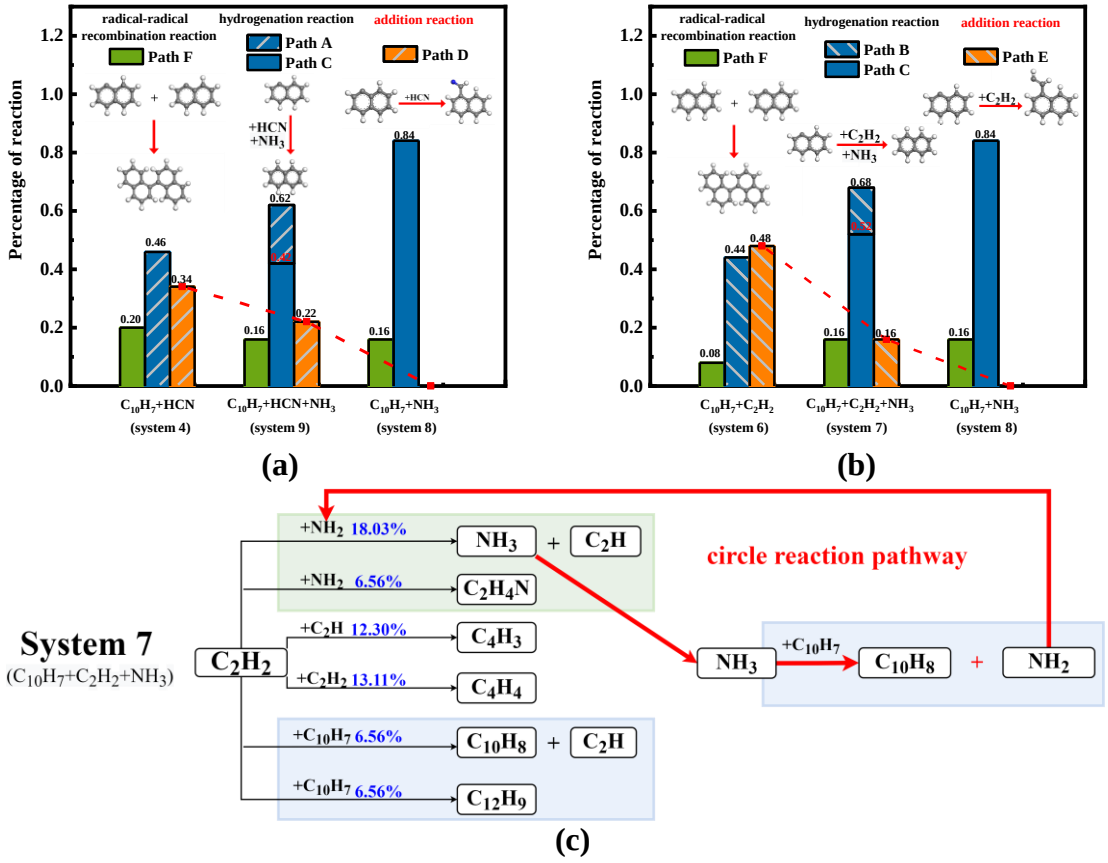

Fig. 7. Percentage of the reaction type of $C_{10}H_7$. Systems of NH_3 added to (a). $C_{10}H_7$/ HCN. (b). $C_{10}H_7$/ C_2H_2 (Green for radical-radical recombination reactions, blue for hydrogenation reactions and orange for addition reactions, shaded part for the reaction with HCN or C_2H_2, un-shaded part for the reaction with NH_3). (c). Reaction pathway between C_2H_2 and NH_3 in system 7 (Blue shading for the reactions related to $C_{10}H_7$, while green shading for the reaction between NH_3 and C_2H_2).

According to the reaction percentages in systems 7 (50 $C_{10}H_7$+250 C_2H_2+250 NH_3) and 9 (50 $C_{10}H_7$+250 HCN+250 NH_3), the reaction of $C_{10}H_7$ with HCN are more frequent than those of $C_{10}H_7$ with C_2H_2 in both hydrogenation reactions and addition reactions. This can be well explained by the reaction pathways between C_2H_2 and NH_3 shown in Fig. 7(c). Among the reaction pathways involving C_2H_2, the most frequent reaction pathway is shown by the thick arrow in Fig. 7(c). It can be found that NH_2 produced by the hydrogenation reaction of $C_{10}H_7$ with NH_3 can further cause NH_3 formation by the reaction of NH_2 with C_2H_2. And then, NH_3 reacts with $C_{10}H_7$ again. Consequently, the circular reaction pathway significantly increases the proportion of the reactions of $C_{10}H_7$ with NH_3 in the system where C_2H_2 and NH_3 coexist. It should

be noted that the circular reaction pathway is not observed in the system of HCN and NH_3. The detailed reaction pathway analysis of HCN and NH_3 is shown in Supplemental Material.

Furthermore, the morphology of the largest species produced within 500 ps in systems 6 ($C_{10}H_7$/ C_2H_2), 7 ($C_{10}H_7$/ C_2H_2/ NH_3) and 8 ($C_{10}H_7$/ NH_3) are $C_{177}H_{139}$, $C_{89}H_{71}N$ and $C_{30}H_{27}N_3$, respectively, indicating that NH_3 addition significantly decreases the PAH growth. This also happens in the systems of NH_3 added to $C_{10}H_7$/ HCN, where the largest species are $C_{88}H_{49}N_{17}$ ($C_{10}H_7$/ HCN system), $C_{51}H_{37}N_9$ ($C_{10}H_7$/ HCN/ NH_3 system) and $C_{30}H_{27}N_3$ ($C_{10}H_7$/ NH_3 system), respectively. However, the results are attributed to different mechanisms. For the $C_{10}H_7$/ HCN/ NH_3 system, $C_{10}H_7$ reacts preferentially with NH_3 because of lower bond dissociation energy of NH_2-H (435 kJ/mol) than H-CN (502.1 kJ/mol), and the reactions are mostly in the form of hydrogenation reactions to produce a stable $C_{10}H_8$ structure. This leads to only a small portion of $C_{10}H_7$ radicals take addition reactions with HCN. Therefore, the PAH growth process slows down. However, for the $C_{10}H_7$/ C_2H_2/ NH_3 system, NH_3 not only plays the dominant role in the reaction with $C_{10}H_7$ compared to C_2H_2 but also consumes the C_2H_2 through the pathways shown in Fig. 7(c). The dual effects result in a faster decrease in the largest species size in the system.

4. Conclusions

In this study, ReaxFF MD simulations and quantum chemical calculations are conducted to provide insights into the effect of NH_3 addition to hydrocarbons on the PAH precursor formation and PAH growth process from an atomistic perspective for the first time. In the C_2H_4/O_2 system, the simulation results imply that NH_3 addition slows down the formation of large carbon-containing species in the system through producing many small C-N species, especially HCN. The present results confirm that the C-N species prevents carbon atoms from participating in soot precursor formation, thereby reducing soot formation. In addition, in the systems containing $C_{10}H_7$, C_2H_2, and HCN, a new HCN-added PAH growth path is found, but with a lower preference than the conventional HACA path with C_2H_2 addition. Several N-PAHs are produced

through the HCN-added PAH growth, which inhibits the PAH growth process. Further study reveals that the effect of NH_3 addition is more pronounced for the conventional HACA path. This is because the circular reaction pathway significantly increases the proportion of the reactions of $C_{10}H_7$ with NH_3 in the system where C_2H_2 and NH_3 coexist. Overall, the present results provide novel insights into the potential refinement of the mechanism of C-N compounds. In future work, studies employing quantum chemistry and/or ab initio MD are needed to investigate N-PAH more deeply.

5. Acknowledgements

This work was supported by the National Natural Science Foundation of China (Grant No. 51921004). Qian Mao acknowledges the research fellowship from Alexander von Humboldt Foundation.

6. Supplementary material

In this work, supplementary material is submitted along with the manuscript, which involves the validations of the ReaxFF force field, the detailed reaction pathway analysis of HCN and NH_3 and optimized geometries on the $C_{10}H_7$+C_2H_2/HCN potential energy surfaces.

References

[1] Y. Guo, Z. Pan, L. An, J. Power Sources 476 (2020) 228454.
[2] A. Valera-Medina, H. Xiao, M. Owen-Jones, W.I.F. David, P.J. Bowen, Prog. Energy Combust. Sci. 69 (2018) 63-102.
[3] J.H. Lee, S.I. Lee, O.C. Kwon, Int. J. Hydrogen Energy 35 (2010) 11332-11341.
[4] L. Dai, S. Gersen, P. Glarborg, A. Mokhov, H. Levinsky, Combust. Flame 218 (2020) 19-26.
[5] X. Zhang, S.P. Moosakutty, R.P. Rajan, M. Younes, S.M. Sarathy, Combust. Flame 234 (2021).
[6] E.C. Okafor, Y. Naito, S. Colson, A. Ichikawa, T. Kudo, A. Hayakawa, H. Kobayashi, Combust. Flame 187 (2018) 185-198.
[7] S. Liu, C. Zou, Y. Song, S. Cheng, Q. Lin, Energy 175 (2019) 250-258.
[8] Z. An, M. Zhang, W. Zhang, R. Mao, X. Wei, J. Wang, Z. Huang, H. Tan, Fuel 304 (2021) 121370.
[9] M. Zhang, Z. An, X. Wei, J. Wang, Z. Huang, H. Tan, Fuel 291 (2021) 120135.
[10] M.J. Montgomery, H. Kwon, J.A.H. Dreyer, Y. Xuan, C.S. McEnally, L.D. Pfefferle, Proceedings of the Combustion Institute 38 (2021) 2497-2505.

[11] P. Glarborg, J.A. Miller, B. Ruscic, S.J. Klippenstein, Prog. Energy Combust. Sci. 67 (2018) 31-68.
[12] C. Shao, F. Campuzano, Y. Zhai, H. Wang, W. Zhang, S. Mani Sarathy, Combust. Flame, doi:10.1016/j.combustflame.2021.111698(2021).
[13] C. Renard, V. Dias, P.J. Van Tiggelen, J. Vandooren, Proceedings of the Combustion Institute 32 (2009) 631-637.
[14] A.M. Bennett, P. Liu, Z. Li, N.M. Kharbatia, W. Boyette, A.R. Masri, W.L. Roberts, Combust. Flame 220 (2020) 210-218.
[15] H.J. B.S.Haynes, H.Mätzing, H.Gg.Wagner, Symposium (International) on Combustion 19 (1982) 1379-1385.
[16] K. Chenoweth, A.C.T. van Duin, W.A. Goddard, The Journal of Physical Chemistry A 112 (2008) 1040-1053.
[17] C. Ashraf, A.C.T. van Duin, The Journal of Physical Chemistry A 121 (2017) 1051-1068.
[18] S.D. Adri C. T. van Duin, Francois Lorant, and William A. Goddard, (2001).
[19] Z. Tian, Y. Li, L. Zhang, P. Glarborg, F. Qi, Combust. Flame 156 (2009) 1413-1426.
[20] C.W. Bauschlicher, S.R. Langhoff, Chem. Phys. Lett. 177 (1991) 133-138.
[21] B.S. Jursic, Journal of Molecular Structure: THEOCHEM 366 (1996) 103-108.
[22] A.D. Kulkarni, D.G. Truhlar, S. Goverapet Srinivasan, A.C.T. van Duin, P. Norman, T.E. Schwartzentruber, The Journal of Physical Chemistry C 117 (2012) 258-269.
[23] W. Wang, L. Xu, J. Yan, Y. Wang, Fuel 267 (2020) 117121.
[24] M. Döntgen, M.-D. Przybylski-Freund, L.C. Kröger, W.A. Kopp, A.E. Ismail, K. Leonhard, Journal of Chemical Theory and Computation 11 (2015) 2517-2524.
[25] W. Humphrey, A. Dalke, K. Schulten, Journal of Molecular Graphics 14 (1996) 33-38.
[26] Y. Zhao, D.G. Truhlar, Theor. Chem. Acc. 120 (2008) 215-241.
[27] A.W. Jasper, N. Hansen, Proceedings of the Combustion Institute 34 (2013) 279-287.
[28] D. Hou, X. You, Physical Chemistry Chemical Physics 19 (2017) 30772-30780.
[29] M.J. Frisch, G.W. Trucks, H.B. Schlegel, G.E. Scuseria, M.A. Robb, J.R. Cheeseman, G. Scalmani, V. Barone, G.A. Petersson, H. Nakatsuji, X. Li, M. Caricato, A.V. Marenich, J. Bloino, B.G. Janesko, R. Gomperts, B. Mennucci, H.P. Hratchian, J.V. Ortiz, A.F. Izmaylov, J.L. Sonnenberg, Williams, F. Ding, F. Lipparini, F. Egidi, J. Goings, B. Peng, A. Petrone, T. Henderson, D. Ranasinghe, V.G. Zakrzewski, J. Gao, N. Rega, G. Zheng, W. Liang, M. Hada, M. Ehara, K. Toyota, R. Fukuda, J. Hasegawa, M. Ishida, T. Nakajima, Y. Honda, O. Kitao, H. Nakai, T. Vreven, K. Throssell, J.A. Montgomery Jr., J.E. Peralta, F. Ogliaro, M.J. Bearpark, J.J. Heyd, E.N. Brothers, K.N. Kudin, V.N. Staroverov, T.A. Keith, R. Kobayashi, J. Normand, K. Raghavachari, A.P. Rendell, J.C. Burant, S.S. Iyengar, J. Tomasi, M. Cossi, J.M. Millam, M. Klene, C. Adamo, R. Cammi, J.W. Ochterski, R.L. Martin, K. Morokuma, O. Farkas, J.B. Foresman, D.J. Fox, Gaussian 16 Rev. B.01, Wallingford, CT, 2016.
[30] S. Li, Q. Jiang, Y. Qi, D. Zhao, Y. Tang, Q. Liu, Z. Chen, Y. Zhu, B. Dai, H. Song, L. Zhang, J. Hazard. Mater., doi:https://doi.org/10.1016/j.jhazmat.2022.129187(2022) 129187.
[31] A.M. Mebel, A. Landera, R.I. Kaiser, J. Phys. Chem. A 121 (2017) 901-926.
[32] P. Liu, Z. Li, A. Bennett, H. Lin, S.M. Sarathy, W.L. Roberts, Combust. Flame 199 (2019) 54-68.

Declaration of interests

☒ The authors declare that they have no known competing financial interests or personal relationships that could have appeared to influence the work reported in this paper.

☐The authors declare the following financial interests/personal relationships which may be considered as potential competing interests: